Heat Mass Transfer (2010) 46:621–638
DOI 10.1007/s00231-010-0607-5

ORIGINAL

Natural convection in attic-shaped spaces subject to sudden and ramp heating boundary conditions

Suvash C. Saha · John C. Patterson · Chengwang Lei

Received: 29 December 2009 / Accepted: 22 April 2010 / Published online: 13 May 2010

Abstract In this study, a discussion of the fluid dynamics in the attic space is reported, focusing on its transient response to sudden and linear changes of temperature along the two inclined walls. The transient behaviour of an attic space is relevant to our daily life. The instantaneous and non-instantaneous (ramp) heating boundary condition is applied on the sloping walls of the attic space. A theoretical understanding of the transient behaviour of the flow in the enclosure is performed through scaling analysis. A proper identification of the timescales, the velocity and the thickness relevant to the flow that develops inside the cavity makes it possible to predict theoretically the basic flow features that will survive once the thermal flow in the enclosure reaches a steady state. A time scale for the heating-up of the whole cavity together with the heat transfer scales through the inclined walls has also been obtained through scaling analysis. All scales are verified by the numerical simulations.

List of symbols

A	Slope of the attic
g	Acceleration due to gravity
h	Height of the attic
k	Thermal conductivity
L	Length of one inclined side of the roof
l	Horizontal half length of the attic
Nu	Nusselt number
Nu_s	Steady state Nusselt number
Nu_{sr}	Nusselt number at quasi-steady state
Nu_h	Nusselt number at quasi-steady mode
p	Pressure
$\hat{p}$	Dimensionless pressure
Pr	Prandtl number
Ra	Rayleigh number
T	Temperature
T_0	Reference temperature
T_c	Cooling temperature
T_h	Heating temperature
t	Time
t_f	Heating up time for sudden heating
t_s	Steady state time
t_{sr}	Quasi-steady time
t_p	Ramp time
u, v	Velocity components
$\hat{u}, \hat{v}$	Dimensionless velocity components
u_r	Unsteady velocity scale
u_q	Velocity scale at quasi-steady state
u_s	Steady state velocity
$\hat{u}_r$	Dimensionless unsteady velocity scale
$\hat{u}_s$	Dimensionless steady-state velocity
u_{sr}	Quasi-steady velocity
$\hat{u}_{sr}$	Dimensionless quasi-steady velocity
V	Volume
x, y	Coordinates
$\hat{x}, \hat{y}$	Dimensionless coordinates

Greek symbols

β	Thermal expansion coefficient
ΔT	Temperature difference between hot surface and the ambient
δ_T	Thickness of the thermal boundary layer
δ_{Ts}	Steady state thickness of the thermal boundary layer

S. C. Saha (✉)
School of Engineering and Physical Sciences,
James Cook University, Townsville, QLD 4811, Australia
e-mail: s_c_saha@yahoo.com

J. C. Patterson · C. Lei
School of Civil Engineering, The University of Sydney,
Sydney, NSW 2006, Australia

δ_{Tr} Thickness of the thermal boundary layer at quasi-steady time
δ_{Tq} Thickness of the thermal boundary layer at the quasi-steady stage
δ_p Thickness of the thermal boundary layer when ramp is finished
δ_T^* Dimensionless thickness of the thermal boundary layer
δ_{Tr}^* Dimensionless thickness of the thermal boundary layer at quasi-steady time
δ_{Tq}^* Dimensionless thickness of the thermal boundary layer at quasi-steady mode
κ Thermal diffusivity
ϕ Angle
ρ Density
v Kinematic viscosity
θ Dimensionless temperature
τ Dimensionless time
τ_r Dimensionless heating-up time ($\tau_r > \tau_p$)
$\tau_{r'}$ Dimensionless heating-up time ($\tau_r < \tau_p$)
τ_s Dimensionless steady-state time
τ_f Dimensionless heating-up time
τ_p Dimensionless ramp time
τ_{sr} Dimensionless quasi-steady time

1 Introduction

Heat transfer through an attic space into or out of buildings is an important issue for attic shaped houses in both hot and cold climates. One of the important objectives for design and construction of houses is to provide thermal comfort for occupants. In the present energy-conscious society, it is also a requirement for houses to be energy efficient, i.e. the energy consumption for heating or air-conditioning houses must be minimized. Relevant to these objectives, research into heat transfer in attics has been conducted for more than two decades. Initially, the focus of the research was to obtain previously unavailable heat transfer data for a triangular enclosure heated or cooled from below. Flack [1] adopted an isosceles triangle for his experimental model and conducted flow visualizations and heat transfer measurements for night-time (heating from below) conditions. The velocity measurements were made primarily to aid the general understanding of the flow structure. It was found that, at low Rayleigh numbers, the flow remained laminar. However, as the Rayleigh number was increased, the flow eventually became turbulent. Flack [1] reported that the transition from laminar to turbulent regimes took place at critical Rayleigh numbers $Ra_c = 2.17 \times 10^5$, 6.39×10^5, and 7.56×10^5 for aspect ratios $A = 0.58$, 1.0 and 1.73, respectively.

The attic space problem under daytime conditions has received very limited attention. The boundary conditions for day-time or summer-time are that the sloping walls of the attic space are isothermally heated and the bottom surface is cooled. Flack [1] first investigated the daytime boundary conditions on the triangular enclosures. The author found that under these conditions, the flow inside the enclosure remained laminar for Rayleigh numbers up to 4.9×10^7. It was found that the resulting heat transfer data could be correlated with heat fluxes calculated for one-dimensional conduction, suggesting that the heat transfer through the enclosure was dominated by conduction. Under the daytime conditions, the heat transfer rates and flow velocities were significantly lower than those under the night-time conditions. Latter Akinsete and Coleman [2] numerically simulated the attic space with a hot upper sloping wall and cooled base. Their aim was to obtain previously unavailable heat transfer data, relevant to air conditioning calculations. This study considered only half of the domain. The authors considered two forms of heating on the hot wall including isothermal heating and constant heat flux heating. The calculated flow remained laminar in this study, which agrees with Flack's [1] experiment for daytime conditions.

With the continuation of the previous work for air conditioning calculation, Asan and Namli [3] reported results for steady, laminar, two-dimensional natural convection in a pitched roof of triangular cross-section under the summer day boundary condition. The results showed that the height-to-base ratio has a profound influence on the temperature and flow field. On the other hand, the effect of Rayleigh number is not significant for $H/B < 1$ and $Ra < 10^5$. For small Rayleigh numbers, two counter rotating vortices are present in the enclosure and the eye of the vortices is located at the center of the half of the cross-section. With the increase of the Rayleigh number, a secondary vortex developed and the newly develop secondary vortex pushes the eye of the primary vortex further towards the inclined wall. The transition from a two-vortex solution to a multiple vortex solution is dependent on the Rayleigh number and the height-to-base ratio.

Scaling analysis of the transient flow inside the attics space has been studied for the case of night time boundary condition by Poulikakos and Bejan [4] with the assumption that the flow is symmetric about the center plane. The authors also assume that the aspect ratio is very small ($A \to 0$) and the working fluid is water. Scaling analyses coupled with numerical simulations have been used in a variety of other geometries and thermal forcing. Recently Lin et al. [5, 6] and Lin and Armfield [7, 8] investigated the transient processes in the cooling of an initially homogeneous fluid by natural convection in a vertical circular cylinder and in a rectangular container for $Pr < 1$. To

identify possible flow regimes of the unsteady natural convection flow in a small-slope shallow wedge induced by the absorption of solar radiation, Lei and Patterson [9] presented a scaling analysis and established relevant scales to quantify the flow properties in each flow regime. A night time cooling boundary condition has been considered for the same geometry by Lei and Patterson [10]. The authors develop some important flow regimes of the boundary layer development.

Patterson et al. [11] consider the ramp heating boundary condition to perform the scaling analysis for natural convection adjacent to the vertical flat plate. The authors considered the working fluid as water ($Pr > 1$). Saha et al. [12, 13] has been studied scaling analysis for the transient development of the fluid flow adjacent to the inclined plate for air ($Pr < 1$) and a range of aspect ratios and Rayleigh numbers. The authors also applied those results for the attic space problem of night time cooling case.

The objective of this study is to understand the phenomenon of thermal convection in an attic or a wedge-shaped space, filled with a Newtonian fluid (air). We investigate the fluid dynamics in the attic space. The main focus has been given to the transient response to sudden and linear changes of temperature along two inclined walls. Certain periods of the day or night may be considered as having a constant ambient temperature (e.g. during 11 a.m.–2 p.m. or 11 p.m.–2 a.m.). However, at other times during the day or night the ambient temperature changes with time (e.g. between 5 a.m. and 9 a.m. or 5 p.m. and 9 p.m.). Based on these natural scenarios, we consider two cases in this study: one with sudden heating on the roof of the attic and the other with ramp heating under which the temperature on the roof follows a ramp function up until a specified temperature and then remains constant.

2 Problem formulations

Under consideration is a triangular cavity of height h, half length of the base l, containing a Newtonian fluid with $Pr < 1$ which is initially at rest with a temperature T_c. At the time $t = 0$, two possible heating boundary conditions are considered on the inclined walls: sudden heating to a specified temperature which is then maintained; and heating by a linearly increasing temperature to a specified temperature over some time (the ramp time) after which the temperature is maintained (the ramp function). In order to avoid the singularities at the tips in the numerical simulation, the tips are cut off by 5% and at the cutting points (refer to Fig. 1) rigid non-slip and adiabatic vertical walls are assumed. The bottom surface is also considered as adiabatic and rigid non-slip. We anticipate that this modification of the geometry will not alter the overall flow development significantly.

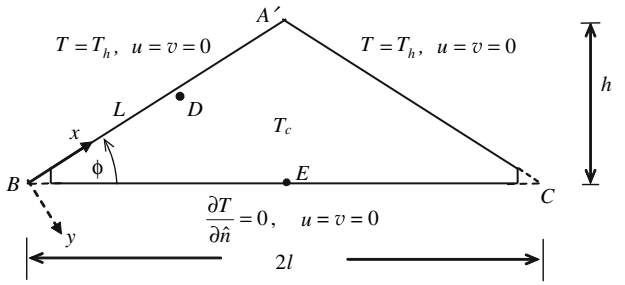

Fig. 1 The schematic of the geometry and the coordinate system of $h/l = 0.5$

The development of natural convection inside an attic space is governed by the following two-dimensional Navier–Stokes and energy equations with the Boussinesq approximation:

$$\frac{\partial u}{\partial x} + \frac{\partial v}{\partial y} = 0 \tag{1}$$

$$\frac{\partial u}{\partial t} + u\frac{\partial u}{\partial x} + v\frac{\partial u}{\partial y} = -\frac{1}{\rho}\frac{\partial p}{\partial x} + \nu\left(\frac{\partial^2 u}{\partial x^2} + \frac{\partial^2 u}{\partial y^2}\right) + g\sin\phi\beta(T - T_c) \tag{2}$$

$$\frac{\partial v}{\partial t} + u\frac{\partial v}{\partial x} + v\frac{\partial v}{\partial y} = -\frac{1}{\rho}\frac{\partial p}{\partial y} + \nu\left(\frac{\partial^2 v}{\partial x^2} + \frac{\partial^2 v}{\partial y^2}\right) + g\cos\phi\beta(T - T_c) \tag{3}$$

$$\frac{\partial T}{\partial t} + u\frac{\partial T}{\partial x} + v\frac{\partial T}{\partial y} = \kappa\left(\frac{\partial^2 T}{\partial x^2} + \frac{\partial^2 T}{\partial y^2}\right) \tag{4}$$

The initial and boundary conditions are defined as follows:

- On the sloping walls a rigid non-slip wall boundary condition is applied. For the sudden heating case, a constant temperature condition, $T = T_h$ and for the ramp heating case the following temperature condition is applied on the slopping walls.

$$T_h = \begin{cases} T_c & \text{if } t \le 0; \\ T_c + \Delta T(t/t_p) & \text{if } 0 < t < t_p; \\ T_c + \Delta T & \text{if } t \ge t_p; \end{cases} \tag{5}$$

  where $\Delta T = T_h - T_c$ and t_p is the time duration of ramp heating.
- The bottom horizontal wall is adiabatic ($\partial T/\partial n = 0$, where n is the direction normal to the wall) and rigid non-slip.
- At the cutting points of the bottom tips rigid non-slip and adiabatic vertical walls are assumed.
- Initially the fluid is motionless and isothermal at temperature T_c.

3 Scaling analysis for sudden heating

In this section we focus on the flow which is dominated by two distinct stages of development, i.e. a boundary-layer development stage and a heating-up stage. The boundary layer development stage is the early stage of the flow development and the heating up stage is the stage when the cavity is filled with hot fluid.

The scaling results of the boundary layer development adjacent to the sloping walls of the attic space are identical to those obtained by Saha et al. [12] for the case of a heated inclined flat plate. Initially the thermal boundary layer adjacent to the sloping wall grows according to $\delta_T \sim \kappa^{1/2}t^{1/2}$.

The ratio of the advection term $O(u^2/L)$ to the unsteady term $O(u/t)$ is $O(ut/L)$. For very small time $ut/L \ll 1$. Therefore, the advection term is insignificant at this time. Again the ratio of the unsteady to viscous term is $(u/t)/(\nu u/\delta_T^2) \sim 1/Pr$, where $Pr = \nu/\kappa$. If $Pr \sim O(1)$, then the unsteady and viscous terms are of the same order, and thus both terms need to be included in a balance with the buoyancy term. Now the balance in the inclined momentum equation is

$$(1+Pr)\frac{u}{t} \sim g\beta\Delta T \sin\phi \tag{6}$$

Therefore $u \sim g\beta \sin\phi \Delta T t/(1+Pr)$. The inclination angle, ϕ is related to the slope or aspect ratio, A through $\sin\phi = A/(1+A^2)^{1/2}$.

The transient velocity scale for the case of sudden heating boundary condition on the inclined flat plate is given by

$$u \sim \frac{ARaPr}{(1+Pr)(1+A^2)^{1/2}}\left(\frac{t}{h^2/\kappa}\right)\left(\frac{\kappa}{h}\right), \tag{7}$$

where $Ra = g\beta\Delta T h^3/(\nu\kappa)$. As time passes, the thermal boundary layer thickness, δ_T continues to grow until a balance between convection and conduction is reached. i.e.

$$u\frac{\Delta T}{L} \sim \kappa\frac{\Delta T}{\delta_T^2} \tag{8}$$

Therefore, the steady state time, thermal layer thickness and the velocity scales using (7) and $\delta_T \sim \kappa^{1/2}t^{1/2}$ are given by

$$t_s \sim \frac{(1+Pr)^{1/2}(1+A^2)^{1/2}}{ARa^{1/2}Pr^{1/2}}\left(\frac{h^2}{\kappa}\right), \tag{9}$$

$$\delta_T \sim \frac{h(1+Pr)^{1/4}(1+A^2)^{1/4}}{A^{1/2}Ra^{1/4}Pr^{1/4}}, \tag{10}$$

and

$$u_s \sim \frac{Ra^{1/2}Pr^{1/2}}{(1+Pr)^{1/2}}\left(\frac{\kappa}{h}\right). \tag{11}$$

In addition to these scaling results, the scaling for heat transfer through the inclined wall of the attic space at the steady state time, in the form of a Nusselt number, have been developed as follows.

3.1 Heat transfer scales

The instantaneous local Nusselt number during the boundary-layer development stage can be calculated as

$$Nu \sim \frac{\left(\frac{\partial T}{\partial y}\right)}{\frac{\Delta T}{h}} \sim \frac{\Delta T}{\delta_T} \times \frac{h}{\Delta T} \sim \frac{h}{\delta_T} \sim \frac{h}{\kappa^{1/2}t^{1/2}}. \tag{12}$$

Using (9), the average steady-state Nusselt number for the boundary layer is given by

$$Nu_s \sim \frac{1}{L}\int_0^L Nu dx \sim \frac{A^{1/2}Ra^{1/4}Pr^{1/4}}{(1+Pr)^{1/4}(1+A^2)^{1/4}}. \tag{13}$$

3.2 Heating up stage

Once the boundary layer is fully developed, the interior of the enclosure is gradually stratified by the hot fluid ejected from the boundary layer, starting from the top of the cavity, and this heating-up stage continues until the hot fluid layer from the top reaches the bottom surface. The appropriate parameters to characterize this heating-up stage are the time, t_f for the fluid to be fully heated-up and the average Nusselt number on the heated wall.

Let us consider an arbitrary moment, t during the heating-up stage. At this moment, the fluid inside the enclosure can be assumed to consist of two layers with the location $x = x_i$ as the interface. The bottom layer is at the original temperature, T_c whereas the top layer is filled with the hot fluid discharged from the thermal boundary layer, the temperature of which is assumed to be the same as the wall temperature T_h.

From $\Delta A'B'C$ and $\Delta A'DE$ in Fig. 2, we have,

$$\frac{L-x_i}{L} = \frac{h-h_i}{h} \Rightarrow h - h_i = h\left(1-\frac{x_i}{L}\right), \tag{14}$$

and

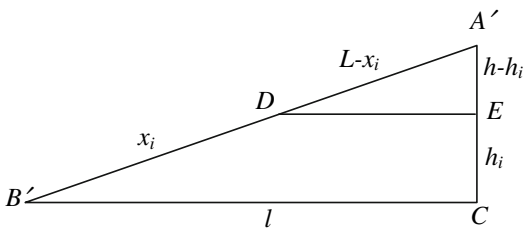

Fig. 2 Schematic of heating-up process for sudden heating

$$\frac{L}{L-x_i}=\frac{l}{DE}\Rightarrow DE=l\left(1-\frac{x_i}{L}\right) \tag{15}$$

Therefore

$$\Delta A'DE=\frac{1}{2}hl\left(1-\frac{x_i}{L}\right)^2\sim\frac{h^2}{A}\left(1-\frac{x_i}{L}\right)^2. \tag{16}$$

Suppose the total volume of the enclosure ABC is

$$V_{\text{total}}=\frac{1}{2}lh. \tag{17}$$

At the steady state time the volume filled by the hot fluid is

$$V_{\text{steady}}\sim u_s\delta_T t_s, \tag{18}$$

which gives

$$V_{\text{steady}}\sim\frac{h^2(1+Pr)^{1/4}(1+A^2)^{3/4}}{A^{3/2}Ra^{1/4}Pr^{1/4}}. \tag{19}$$

The ratio of the volumes

$$\frac{V_{\text{steady}}}{V_{\text{total}}}\sim\frac{(1+Pr)^{1/4}(1+A^2)^{3/4}}{A^{1/2}Ra^{1/4}Pr^{1/4}}. \tag{20}$$

It is estimated that the maximum ratio of the volume filled by hot fluid during the transient stage (from start-up to the steady state time) to the total volume of the enclosure is less than 0.095 over the ranges of Ra, A and other parameters considered here. Therefore, the filled volume at the transient stage is insignificant compared to the total volume and is neglected below.

From the mass conservation law

$$\frac{h^2}{A}\left(1-\frac{x_i}{L}\right)^2\sim u_s\delta_T t. \tag{21}$$

Now applying (7) and (8) in (18) we have,

$$\frac{h^2}{A}\left(1-\frac{x_i}{L}\right)^2\sim\frac{\kappa(1+A^2)^{1/4}Ra^{1/4}\,\mathrm{Pr}^{1/4}}{(1+Pr)^{1/4}A^{1/2}}t$$

$$\Rightarrow x_i\sim L\left[1-\frac{\kappa^{1/2}A^{1/4}Ra^{1/8}Pr^{1/8}(1+A^2)^{1/8}}{h(1+Pr)^{1/8}}t^{1/2}\right]. \tag{22}$$

The time when the whole enclosure is filled with hot fluid ($x_i\sim 0$) is obtained as

$$t_f\sim\frac{(1+Pr)^{1/4}}{A^{1/2}Ra^{1/4}Pr^{1/4}(1+A^2)^{1/4}}\left(\frac{h^2}{\kappa}\right). \tag{23}$$

Since only the lower part of the sloping wall contributes to the heat transfer at any given time, it is apparent from (9) that the instantaneous global Nusselt number, Nu at the heating up stage is,

$$Nu\sim\left(\frac{x_i}{L}\right)Nu_s. \tag{24}$$

Applying (22) and (23) in (24), we have

$$\frac{Nu}{Nu_s}\sim 1-\frac{\kappa^{1/2}A^{1/4}Ra^{1/8}Pr^{1/8}}{h(1+Pr)^{1/8}}t^{1/2}$$

$$\Rightarrow\frac{Nu}{Nu_s}\sim 1-\left(\frac{t}{t_f}\right)^{1/2}. \tag{25}$$

4 Scaling analysis for ramp heating

Like sudden heating case, a detail of scaling results for the case with the ramp heating temperature boundary condition has been produced in Saha et al. [12] for an inclined thermal boundary layer. As soon as the heating boundary condition applied on the inclined wall, a thermal boundary layer starts to develop with the scale $\kappa^{1/2}t^{1/2}$. By balancing the unsteady and viscous terms with the buoyancy term the transient velocity scale inside the boundary layer is given by

$$u_r\sim\frac{ARaPr}{(1+Pr)(1+A^2)^{1/2}}\left(\frac{t}{h^2/\kappa}\right)\left(\frac{t}{t_p}\right)\left(\frac{\kappa}{h}\right). \tag{26}$$

This scale is valid until the quasi-steady time if the ramp time is larger than the quasi-steady time or until the ramp is finished if the ramp time is shorter than the steady state time.

It is shown in Saha et al. [12] that for the case of inclined flat plate the steady state scales for the ramp heating boundary condition of time, velocity and the boundary layer thickness are exactly the same as those for the sudden heating boundary condition if the ramp time is shorter than the steady state time. However, if the quasi-steady time is shorter than the ramp time ($t_{sr}<t_p$), then by balancing the unsteady and viscous terms with the buoyancy term we get the quasi-steady time (t_{sr}), the thermal layer thickness (δ_{Tr}) and velocity scales (u_{sr}) are given, respectively, by

$$t_{sr}\sim\frac{(1+Pr)^{1/3}(1+A^2)^{1/3}}{A^{2/3}Ra^{1/3}Pr^{1/3}}\left(\frac{t_p}{h^2/\kappa}\right)^{1/3}\left(\frac{h^2}{\kappa}\right), \tag{27}$$

$$\delta_{Tr}\sim\frac{h(1+Pr)^{1/6}(1+A^2)^{1/6}}{A^{1/3}(RaPr)^{1/6}}\left(\frac{t_p}{h^2/\kappa}\right)^{1/6}, \tag{28}$$

and

$$u_{sr}\sim\frac{(RaPr)^{1/3}(1+A^2)^{1/6}}{A^{1/3}(1+Pr)^{1/3}}\left(\frac{h^2/\kappa}{t_p}\right)^{1/3}\left(\frac{\kappa}{h}\right). \tag{29}$$

After the quasi-steady time the thermal boundary layer develops according to the scale in the quasi-steady mode

$$\delta_{Tq}\sim\frac{h(1+A^2)^{1/4}}{A^{1/2}Ra^{1/4}}\left(\frac{t_p}{t}\right)^{1/4}, \tag{30}$$

and the velocity grows according to the scale

$$u_q \sim Ra^{1/2}\left(\frac{\kappa}{h}\right)\left(\frac{t}{t_p}\right). \tag{31}$$

These two scales are valid until the ramp is finished. After the ramp is finished the boundary layer does not know that it comes from a ramp function.

In addition of those, for the attic space, a heat transfer scaling at different times of boundary layer development in a form of a Nusselt number has been developed as follows:

4.1 Heat transfer scaling for ramp heating

Since initially the temperature on the inclined wall changes with time, the temperature difference between the wall and the interior is also changing with time up to the time when the ramp is finished. Therefore, the temperature difference is constant (maximum) after the ramp is finished. We may consider the maximum temperature difference or the transient temperature difference in the Nusselt number definition. Firstly, if we consider the temperature difference, ΔT as the maximum then the local Nusselt number on the inclined surface during the boundary-layer development stage is

$$Nu_X \sim \frac{\left(\frac{\partial T}{\partial y}\right)}{\frac{\Delta T}{h}} \sim \frac{\Delta T}{\delta_T} \times \frac{h}{\Delta T} \sim \frac{h}{\delta T} \sim \frac{h}{\kappa^{1/2} t^{1/2}}. \tag{32}$$

Using (27), the average quasi-steady state Nusselt for the whole boundary layer is given by

$$Nu_{sr} \sim \frac{1}{L}\int_0^L Nu_X dx \sim \frac{A^{1/3} Ra^{1/6} Pr^{1/6}}{(1+Pr)^{1/6}(1+A^2)^{1/6}}\left(\frac{h^2/\kappa}{t_p}\right)^{1/6}. \tag{33}$$

After the quasi-steady state time, the boundary layer does not grow as $\kappa^{1/2}t^{1/2}$. It grows according to the scale (30). Therefore, the Nusselt number at the quasi-steady state mode is

$$Nu_h \sim \frac{A^{1/2} Ra^{1/4}}{(1+A^2)^{1/4}}\left(\frac{t}{t_p}\right)^{1/4}. \tag{34}$$

However, if we consider the instantaneous temperature difference then the local Nusselt number on the inclined surface during the boundary-layer development stage is

$$Nu_X \sim \frac{\left(\frac{\partial T}{\partial y}\right)}{\frac{\Delta T}{h}} \sim \frac{\Delta T t}{\delta_T t_p} \times \frac{h}{\Delta T} \sim \frac{ht}{\delta_T t_p} \sim \frac{ht^{1/2}}{\kappa^{1/2} t_p}. \tag{35}$$

At the quasi-steady state time predicted by (27), the local Nusselt number is

$$Nu_{ins} \sim \frac{1}{L}\int_0^L Nu_X dx \sim \frac{(1+Pr)^{1/6}(1+A^2)^{1/6}}{A^{1/3} Ra^{1/6} Pr^{1/6}}\left(\frac{h^2/\kappa}{t_p}\right)^{5/6}. \tag{36}$$

Similarly to (34), we may derive the Nusselt number at the quasi-steady state mode as

$$Nu_h \sim \frac{A^{1/2} Ra^{1/4}}{(1+A^2)^{1/4}}\left(\frac{t}{t_p}\right)^{5/4}. \tag{37}$$

4.2 Heating up scale of the entire cavity

Similarly to the sudden heating case, once the boundary layer is fully developed by the ramp heating on the sloping boundary, the fluid in the enclosure is gradually stratified by the hot fluid ejected from the boundary layer, starting from the top of the cavity, and this heating up stage continues until the whole body of fluid has the same temperature as that imposed on the incline walls of the attic space. The appropriate parameters characterizing this heating up stage are the time, t_f for the fluid to be fully heated up and the average Nusselt number on the heating wall.

Let us consider an arbitrary moment t during the heating up stage. At that moment, the fluid inside the enclosure is assumed to consist of two layers with the location $x = x_i$ as the interface. The bottom layer is at the original temperature, T_c, whereas the top layer is at the wall temperature T_h.

The total volume of the enclosure $A'B'C$ is (see Fig. 3)

$$V_{\text{total}} = \frac{1}{2} lh. \tag{38}$$

At the quasi-steady state time the volume filled by the hot fluid is

$$V_{\text{steady}} \sim u_{sr}\delta_{Tr} t_{sr}. \tag{39}$$

which gives

$$V_{\text{steady}} \sim \frac{h^2(1+Pr)^{1/6}(1+A^2)^{2/3}}{A^{4/3} Ra^{1/6} Pr^{1/6}}\left(\frac{t_p}{h^2/\kappa}\right)^{1/6}. \tag{40}$$

The ratio of the above two volumes is

$$\frac{V_{\text{steady}}}{V_{\text{total}}} \sim \frac{(1+Pr)^{1/6}(1+A^2)^{2/3}}{A^{1/3} Ra^{1/6} Pr^{1/6}}\left(\frac{t_p}{h^2/\kappa}\right)^{1/6}. \tag{41}$$

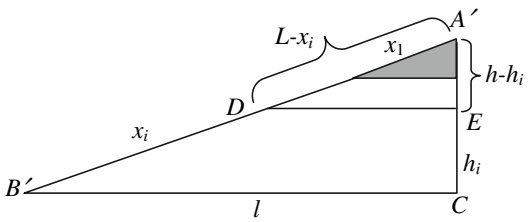

Fig. 3 Schematic of heating-up process for ramp heating

The maximum ratio of the volume filled with hot fluid at the transient stage to the total volume of the cavity is less than 0.08 for the ranges of Ra, A and other parameters considered here. Therefore, the quasi-steady time can be ignored for the calculation of the filling box time.

Suppose the ramp is finished when the interface is at $x = x_1$ measured from A, for the case when the ramp time is longer than the quasi-steady time ($t_p > t_{sr}$). Let us calculate the volume of the hot portion filled by the time $t = t_p$. The volume of the heated portion is

$$V_1 = \frac{1}{2} lh\left(\frac{x_1}{L}\right)^2. \tag{42}$$

The flux at the time $t = t_p$ is

$$u_q \delta_T t|_{t=t_p} = \frac{\kappa A^{1/2} Ra^{1/4} (1+A^2)^{1/4}}{h^2} t_p. \tag{43}$$

Mass conservation then requires

$$\frac{1}{2} lh\left(\frac{x_1}{L}\right)^2 \sim \frac{\kappa Ra^{1/4}(1+A^2)^{1/4}}{A^{1/2}} t_p$$
$$\Rightarrow x_1 \sim L\left[\frac{\kappa A^{1/2} Ra^{1/4}(1+A^2)^{1/4}}{h^2} t_p\right]^{1/2}. \tag{44}$$

Therefore, the volume, V_1 is filled up with hot fluid by the time $t = t_p$. The rest of the volume will be filled up after the ramp is finished. At $t = t_p$ the thermal boundary layer thickness and the velocity scales from (30) and (31), respectively, are

$$\delta_p \sim \frac{h(1+A^2)^{1/4}}{A^{1/2} Ra^{1/4}}, \tag{45}$$

and

$$u_p = Ra^{1/2}\left(\frac{\kappa}{h}\right) \tag{46}$$

The rest of the volume after ramp is finished is

$$\frac{1}{2} lh\left(1 - \frac{x_i}{L}\right)^2 - \frac{1}{2} lh\left(\frac{x_1}{L}\right)^2 \sim \frac{A}{1+A^2}\left[(L-x_i)^2 - x_1^2\right].$$

Again from the mass conservation law we have

$$\frac{A}{1+A^2}\left[(L-x_i)^2 - x_1^2\right] \sim u_\rho \delta_\rho t. \tag{47}$$

Applying (45) and (46) we have,

$$\frac{A}{1+A^2}\left[(L-x_i)^2 - x_1^2\right] \sim \frac{\kappa Ra^{1/4}(1+A^2)^{1/4}}{A^{1/2}} t$$
$$\Rightarrow x_i \sim L - \left[x_1^2 + \frac{\kappa Ra^{1/4}(1+A^2)^{5/4}}{A^{3/2}} t\right]^{1/2}. \tag{48}$$

Recognizing that for $t = t_r$, $x_i = 0$, therefore,

$$t_r \sim \frac{\left[h^2(1+A^2) - A^2 x_1^2\right]}{A^{1/2}\kappa Ra^{1/4}(1+A^2)^{5/4}}, \tag{49}$$

where $L = (h/A)(1 + A^2)^{1/2}$.

However, if the enclosure is heated up before the ramp is finished then

$$\frac{h^2}{2A}\left(1 - \frac{x_i}{L}\right)^2 \sim u_{sr}\delta_{sr} t. \tag{50}$$

Applying (29) and (28) we have,

$$\Rightarrow x_i \sim L\left[1 - \frac{\kappa^{5/12}(1+A^2)^{1/6} A^{1/6} (RaPr)^{1/12}}{h^{5/6}(1+Pr^2)^{1/12} t_p^{1/12}} t^{1/2}\right]. \tag{51}$$

and the heating-up time is then given by

$$t_{r'} \sim \frac{(1+Pr)^{1/6} t_p^{1/12}}{(1+A^2)^{1/3} A^{1/3} (RaPr)^{1/6}} \left(\frac{t_p}{h^2/\kappa}\right)^{1/6} \left(\frac{h^2}{\kappa}\right). \tag{52}$$

It is apparent from (33) that the instantaneous Nusselt number, Nu at the heating up stage is

$$Nu \sim \left(\frac{x_i}{L - x_1}\right) Nu_p \tag{53}$$

Using (48) and (49), we have

$$\frac{Nu}{Nu_p} \sim 1 - \left(\frac{t}{t_r}\right)^{1/2} \text{for } t > t_p, \tag{54}$$

where Nu_p is the Nusselt number at the time, $t = t_p$

$$Nu_p \sim \frac{Ra^{1/4} A^{1/2}}{(1+A^2)^{1/4}} \tag{55}$$

In the following sections, the above scaling relations are validated against the numerical simulation. However, grid and the time step dependence tests must first be performed to ensure the accuracy of the numerical results. Two-dimensional numerical simulations have been carried out in this study. For this purpose, an isosceles triangular domain is considered, and a Cartesian coordinate system is adopted, which is shown in Fig. 1.

5 Numerical scheme and grid and time step dependence test

To facilitate the numerical validation of the scalings obtained above, dimensionless forms of the governing equations and the scalings are used. The governing Eqs. 1–4 can be written in the following non-dimensional forms,

$$\frac{\partial \hat{u}}{\partial \hat{x}} + \frac{\partial \hat{u}}{\partial \hat{y}} = 0 \tag{56}$$

$$\frac{\partial \hat{u}}{\partial \tau}+\hat{u}\frac{\partial \hat{u}}{\partial \hat{x}}+\hat{v}\frac{\partial \hat{u}}{\partial \hat{y}}=-\frac{\partial \hat{p}}{\partial \hat{x}}+Pr\left(\frac{\partial^2 \hat{u}}{\partial \hat{x}^2}+\frac{\partial^2 \hat{u}}{\partial \hat{y}^2}\right)+Ra\,Pr\,\theta\sin\phi \tag{57}$$

$$\frac{\partial \hat{v}}{\partial \tau}+\hat{u}\frac{\partial \hat{v}}{\partial \hat{x}}+\hat{v}\frac{\partial \hat{u}}{\partial \hat{y}}=-\frac{\partial \hat{p}}{\partial \hat{y}}+Pr\left(\frac{\partial^2 \hat{v}}{\partial \hat{x}^2}+\frac{\partial^2 \hat{v}}{\partial \hat{y}^2}\right)+Ra\,Pr\,\theta\cos\phi \tag{58}$$

$$\frac{\partial \theta}{\partial \tau}+\hat{u}\frac{\partial \theta}{\partial \hat{x}}+\hat{v}\frac{\partial \theta}{\partial \hat{y}}=\left(\frac{\partial^2 \theta}{\partial \hat{x}^2}+\frac{\partial^2 \theta}{\partial \hat{y}^2}\right) \tag{59}$$

where $\hat{x}$, $\hat{y}$, $\hat{u}$, $\hat{v}$, θ, $\hat{p}$ and τ are, respectively, the normalised forms of x, y, u, v, T, p and t, which are made normalised by the following set of expressions, i.e.,

$$\hat{x}=\frac{x}{h},\quad \hat{y}=\frac{y}{h},\quad \hat{u}=\frac{u}{\kappa/h},\quad \hat{v}=\frac{v}{\kappa/h},\quad \tau=\frac{t}{h^2/\kappa}$$
$$\hat{p}=\frac{p}{\rho\kappa^2/h^2},\quad \theta=\frac{T-T_c}{T_h-T_c} \tag{60}$$

The dimensionless initial and boundary conditions are defined as follows:

- On the sloping walls a rigid non-slip wall boundary condition is applied. For the sudden heating case, a constant temperature condition, $\theta = 1$ and for the ramp heating case the following temperature condition is applied on the slopping walls.

$$\theta=\begin{cases}0 & \text{if } \tau\le 0;\\ (\tau/\tau_p) & \text{if } 0<\tau<\tau_p\\ 1 & \text{if } \ge\tau_p\end{cases} \tag{61}$$

  where τ_p is the time duration of ramp heating.
- The bottom horizontal wall is adiabatic ($\partial\theta/\partial n = 0$, where n is the direction normal to the wall) and rigid non-slip.
- At the cutting points of the bottom tips rigid non-slip and adiabatic vertical walls are assumed.
- Initially the fluid is motionless and isothermal at temperature, $\theta = 0$.

The dimensionless form of selected scales are as follows:

For the sudden heating case the relations (7), (9), (10), (11), (23) and (25) can be written in dimensionless form, respectively, as

$$\hat{u}\sim\frac{u}{\kappa/h}\sim\frac{ARaPr}{(1+Pr)(1+A^2)^{1/2}}\tau \tag{62}$$

$$\tau_s\sim\frac{t}{h^2/\kappa}\sim\frac{(1+Pr)^{1/2}(1+A^2)^{1/2}}{ARa^{1/2}Pr^{1/2}} \tag{63}$$

$$\delta_T^*\sim\frac{\delta_T}{h}\sim\frac{(1+Pr)^{1/4}(1+A^2)^{1/4}}{A^{1/2}Ra^{1/4}Pr^{1/4}} \tag{64}$$

$$\hat{u}_s\sim\frac{u_s}{\kappa/h}\sim\frac{Ra^{1/2}Pr^{1/2}}{(1+Pr)^{1/2}} \tag{65}$$

$$\tau_f\sim\frac{t_f}{h^2/\kappa}\sim\frac{(1+Pr)^{1/4}}{A^{1/2}Ra^{1/4}Pr^{1/4}(1+A^2)^{1/4}} \tag{66}$$

$$\frac{Nu}{Nu_s}\sim 1-\left(\frac{\tau}{\tau_f}\right)^{1/2} \tag{67}$$

For ramp heating case for boundary layer development stage the relations (26), (27), (28), (29), (30) and (31), respectively, as

$$\hat{u}_r\sim\frac{u_r}{\kappa/h}\sim\frac{ARa\,Pr}{(1+Pr)(1+A^2)^{1/2}}\left(\frac{\tau^2}{\tau_p}\right) \tag{68}$$

$$\tau_{sr}\sim\frac{t_{sr}}{h^2/\kappa}\sim\frac{(1+Pr)^{1/3}(1+A^2)^{1/3}}{A^{2/3}Ra^{1/3}Pr^{1/3}}\tau_p^{1/3} \tag{69}$$

$$\delta_{Tr}^*\sim\frac{\delta_{Tr}}{h}\sim\frac{(1+Pr)^{1/6}(1+A^2)^{1/6}}{A^{1/3}Ra^{1/6}Pr^{1/6}}\tau_p^{1/6} \tag{70}$$

$$\hat{u}_{sr}\sim\frac{u_{sr}}{\kappa/h}\sim\frac{Ra^{1/3}Pr^{1/3}(1+A^2)^{1/6}}{A^{1/3}(1+Pr)^{1/3}}\frac{1}{\tau_p^{1/3}} \tag{71}$$

$$\delta_{Tq}^*\sim\frac{\delta_{Tq}}{h}\sim\frac{(1+A^2)^{1/4}}{A^{1/2}Ra^{1/4}}\left(\frac{\tau_p}{\tau}\right)^{1/4} \tag{72}$$

$$\hat{u}_q\sim\frac{u_q}{\kappa/h}\sim Ra^{1/2}\left(\frac{\tau}{\tau_p}\right) \tag{73}$$

and the Nusselt number scales (33), (34) and (36), respectively, are

$$Nu_{sr}\sim\frac{A^{1/3}Ra^{1/6}Pr^{1/6}}{(1+Pr)^{1/6}(1+A^2)^{1/6}}\frac{1}{\tau_p^{1/6}} \tag{74}$$

$$Nu_h\sim\frac{A^{1/2}Ra^{1/4}}{(1+A^2)^{1/4}}\left(\frac{\tau}{\tau_p}\right)^{1/4} \tag{75}$$

$$Nu_{ins}\sim\frac{(1+Pr)^{1/6}(1+A^2)^{1/6}}{A^{1/3}Ra^{1/6}Pr^{1/6}}\frac{1}{\tau_p^{5/6}} \tag{76}$$

For the heating up stage the scales (49), (52) and (54) are, respectively, as

$$\tau_r\sim\frac{t_r}{h^2/\kappa}\sim\frac{\left[(1+A^2)-A^2\hat{x}_1^2\right]}{A^{1/2}Ra^{1/4}(1+A^2)^{5/4}} \tag{77}$$

$$\tau_{r'}\sim\frac{t_{r'}}{h^2/\kappa}\sim\frac{(1+Pr)^{1/6}\tau_p^{1/6}}{A^{1/3}(1+A^2)^{1/3}Ra^{1/6}Pr^{1/6}} \tag{78}$$

$$\frac{Nu}{Nu_p}\sim 1-\left(\frac{\tau}{\tau_r}\right)^{1/2}\quad \text{for } \tau>\tau_p \tag{79}$$

In order to avoid singularities at the tips in the numerical simulation, the tips are cut off by 5%, and an extra rigid

Table 1 Grid distribution for aspect ratio 1.0

Grid (H × L)	In the horizontal direction			In the vertical direction		Time step
	Left (EF)	Middle	Right (EF)	Bottom tip	Symmetry line (EF)	
180 × 60	28 (1.030)	34	28 (1.02)	60	40 (1.030)	4.52×10^{-6}
270 × 90	42 (1.025)	51	42 (1.02)	90	60 (1.025)	3.40×10^{-6}
360 × 120	56 (1.020)	68	56 (1.02)	120	80 (1.020)	2.26×10^{-6}
540 × 180	84 (1.016)	102	84 (1.02)	180	120 (1.016)	1.70×10^{-6}

EF expansion factor, *H* horizontal grid, *L* vertical grid

Table 2 Grid distribution for aspect ratio 0.5

Grid (H × L)	In the horizontal direction			In the vertical direction		Time step
	Left (EF)	Middle	Right (EF)	Bottom tip	Symmetry line (EF)	
160 × 40	25 (1.030)	30	25 (1.02)	40	40 (1.030)	4.52×10^{-6}
240 × 60	38 (1.025)	44	38 (1.02)	60	60 (1.025)	3.40×10^{-6}
320 × 80	50 (1.020)	60	50 (1.02)	80	80 (1.020)	2.26×10^{-6}
480 × 120	75 (1.016)	90	75 (1.02)	120	120 (1.016)	1.70×10^{-6}

Table 3 Grid distribution for aspect ratio 0.2

Grid (H × L)	In the horizontal direction			In the vertical direction		Time step
	Left (EF)	Middle	Right (EF)	Bottom tip	Symmetry line (EF)	
180 × 45	30 (1.030)	30	30 (1.02)	45	45 (1.030)	4.52×10^{-6}
280 × 70	45 (1.025)	50	45 (1.02)	70	70 (1.025)	3.40×10^{-6}
360 × 90	60 (1.020)	60	60 (1.02)	90	90 (1.020)	2.26×10^{-6}
560 × 140	95 (1.016)	90	95 (1.02)	140	140 (1.016)	1.70×10^{-6}

non-slip and adiabatic vertical wall boundary is assumed near each tip. It is anticipated that this modification of the geometry will not alter the overall flow development significantly. Equations 1–4 are solved along with the initial and boundary conditions using the SIMPLE scheme. The finite volume method has been chosen to discretize the governing equations, with the QUICK scheme (see Leonard and Mokhtari [14]) approximating the advection term. The diffusion terms are discretized using central-differencing with second order accurate. A second order implicit time-marching scheme has also been used for the unsteady term

An accurate and reliable numerical result depends on the resolution and distribution of the meshes inside the computational domain. In some regions in the domain we may need to distribute a significant number of meshes in order to resolve true physical flow features (e.g. boundary layers). The results may be inaccurate if the mesh is not distributed properly or the number of mesh nodes inside the domain is insufficient. Unfortunately, it is difficult to accurately determine the locations of significance before the calculation is actually carried out, however, we may use our previous knowledge to locate the regions of large flow gradients. Although an increase in the grid resolution will generally increase the numerical accuracy, it also increases the usage of computing resources for both calculation and post-processing. Therefore, it is necessary to compromise between the numerical accuracy and computing efficiency when considering the grid used for the simulations.

Since the thermal boundary layer develops adjacent to the inclined heated walls of the attic space and the gradients of all parameters are very strong near the two bottom tips, finer meshes need to be distributed near the walls and two bottom tips compared to other regions. An expansion factor may be adopted to distribute the non uniform mesh. However, the expanding factor of grid is usually limited in order to ensure that the solution is not degraded. A factor of up to 10% may be used according to Patterson and Armfield [15].

The distribution of mesh has been shown for three different aspect ratios in Tables 1, 2 and 3. We divide the whole domain into two by the symmetry line. Then both left and right portions of the domain are again divided horizontally into three equal portions. The middle portion of the three sub region is mapped uniformly in the horizontal direction (see Fig. 4), and the other two sub-regions

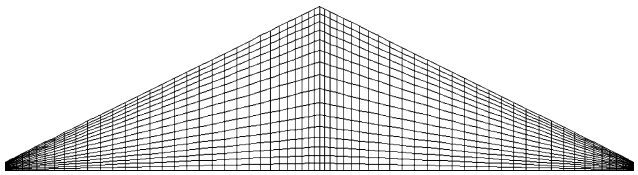

Fig. 4 A sample grid showing the major features of the non-uniform symmetric meshes adopted in this study

are mapped non-uniformly in the horizontal direction. The symmetry line is mapped non-uniformly in the vertical direction with finer meshes near the bottom and apex. However, a uniform mesh has been distributed vertically on two bottom tips (tips are cut by 5%). A schematic of the grid distribution has been shown in Fig. 4.

The initial and boundary conditions for the numerical simulations are also specified as the air in the enclosure is initially motionless and isothermal with a uniform temperature of $\theta = 0$. All the interior surfaces of the enclosure are assumed rigid and no slip.

Grid and time step dependence tests have been conducted for the numerical procedures described earlier for the highest Rayleigh number case for both boundary conditions (sudden heating and ramp heating). It is expected that the mesh selected for the highest Rayleigh number will also be applicable for all lower Rayleigh numbers. The time steps have been chosen in such a way that the CFL (Courant–Freidrich–Lewy) number remains the same for all meshes.

Four different meshes for each aspect ratio, i.e. 180×60, 270×90, 360×120 and 540×180 for $A = 1.0$; 160×40, 240×60, 320×90 and 480×120 for $A = 0.5$ and 180×45, 280×70, 360×90 and 560×140 for $A = 0.2$ have been tested for the case of sudden heating boundary condition.

The time histories of the calculated maximum velocity parallel to the sloping wall for different slopes with the four different meshes are plotted in Fig. 5 for the case of the sudden heating boundary condition. It is seen in the figure that all solutions indicate three stages of the flow development, an initial growth stage, a transitional stage and a steady state stage. In the initial and steady state stage, the four solutions follow each other closely (except for the solution with the coarsest mesh 160×40 for $A = 0.5$, which deviates slightly from the other three meshes in Fig. 5b. The transitional stage is characterized by a single overshoot. The time to reach the steady state is around 2.26×10^{-3}, 1.47×10^{-3} and 7.35×10^{-3} for $A = 1.0$, 0.5 and 0.1, respectively. The maximum variation of the velocity between the coarsest and finest meshes for $A = 0.5$ is 5.35%. However, the maximum variation among the other three finer meshes is only 1.18%. The maximum variations of the velocity between the coarsest and finest meshes for $A = 1.0$ and 0.2 are 0.66 and 1.07%, respectively. Accordingly, the mesh 320×90 for $A = 0.5$ and 360×120 and 360×90 for aspect ratios $A = 1.0$ and 0.2, respectively, are adopted for the present simulations.

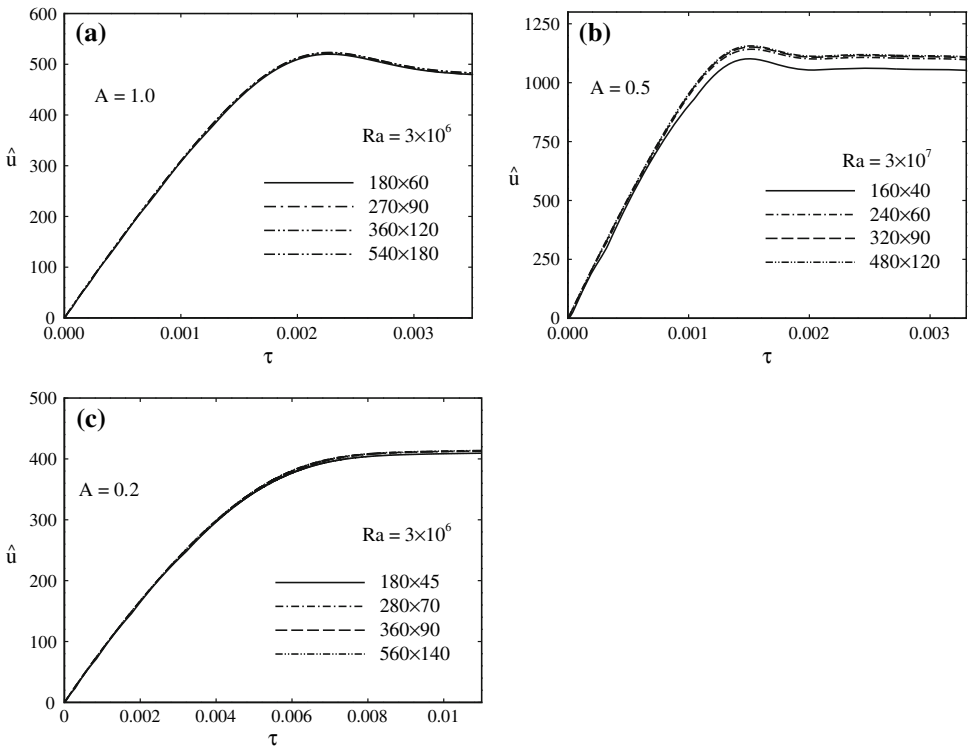

Fig. 5 Maximum velocity parallel to the left inclined wall at its midpoint of four different meshes for each $A = 1.0$, 0.5 and 0.2 and $Pr = 0.72$ for sudden heating

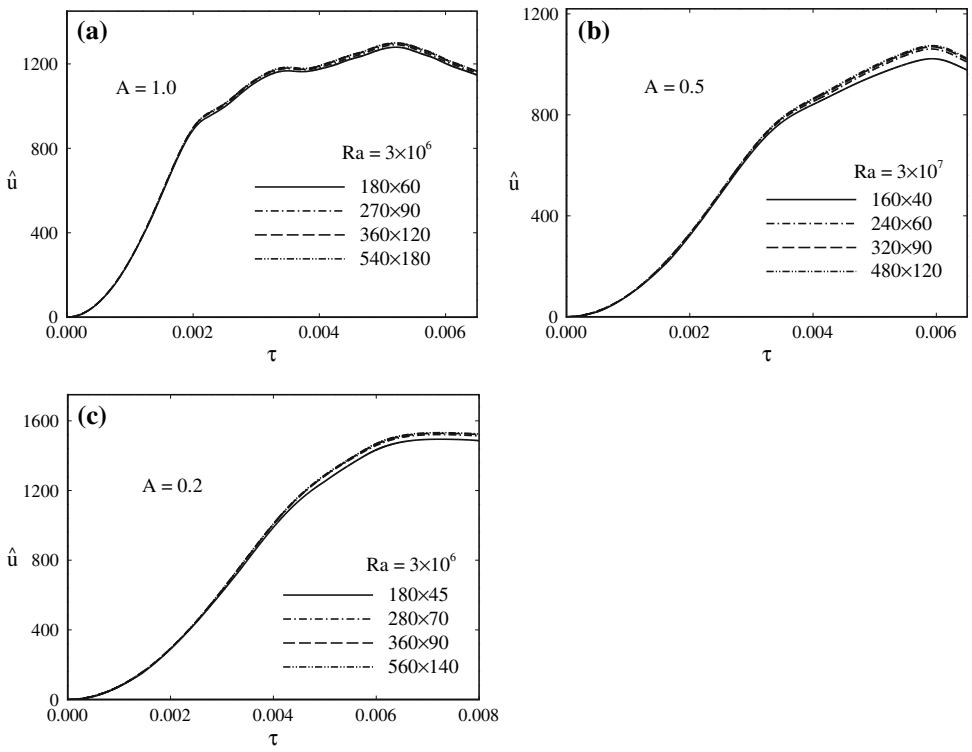

Fig. 6 Maximum velocity parallel to the left inclined wall at its midpoint of four different meshes for each $A = 1.0$, 0.5 and 0.2 and $Pr = 0.72$ for ramp heating

Mesh and time step dependence tests have also been conducted for the ramp heating boundary condition to ensure the accuracy of the numerical solutions. The same meshes as the sudden heating boundary condition have been considered here for three different aspect ratios.

Figure 6 shows the time series of the maximum velocity parallel to the inclined surface calculated on the line normal to the surface at the midpoint for three different aspect ratios under the ramp heating boundary condition for $Pr = 0.72$. These velocities are calculated with four different meshes for each aspect ratio. The ramp time has been set to 5.66×10^{-3} for all the cases. As is mentioned in the scaling analysis, the ramp time may be either longer or shorter than the steady state time for the boundary layer. If the ramp time is longer than the quasi-steady time, then after the quasi-steady time the velocity continues to increase as the inclined wall is still being heated. However, the growth rate of the velocity is smaller than the velocity during the earlier phase. It is seen in this figure that at about 2.04×10^{-3}, 3.11×10^{-3} and 4.3×10^{-3} for $A = 1.0$, 0.5 and 0.2, respectively, the boundary layer becomes quasi-steady. However, the velocity still increases as the temperature on the wall is still increasing. At $\tau = 5.66 \times 10^{-3}$, the ramp finishes and the boundary layer becomes completely steady.

The maximum variation of the velocity between the coarsest and finest meshes for $A = 1.0$ is 1.78%. The maximum variations of the velocity between the coarsest and finest meshes for $A = 0.5$ and 0.2 are 5.78 and 2.55%, respectively. However, the maximum variations among the three fine meshes are 1.29 and 0.75%, for $A = 0.5$ and 0.2, respectively. Accordingly, the mesh size 360×120, 320×90 and 360×90 are adopted for $A = 1.0$, 0.5 and 0.2, respectively for the whole range of simulations.

Four different time steps have been tested along with the four different meshes for each aspect ratio (see Tables 1, 2, 3). The time step size 2.26×10^{-6} has been adopted for simulation for both sudden heating and ramp heating boundary condition. With the selected meshes and time steps, the maximum CFL numbers are 0.013, 0.14 and 0.14 for $A = 0.2$, 0.5 and 1.0, respectively, at the steady stage.

6 Flow development in different regimes for sudden heating

6.1 Conduction regime

The numerical results for a low Rayleigh number have been shown in Fig. 7 with $Pr = 0.72$, $Ra = 10$ and $A = 0.5$ for the regime $Ra < (1 + Pr)(1 + A^2)/(A^2 Pr)$. The temperature contours and streamlines at $\tau/\tau_s = 0.156$ are plotted in Fig. 9a, b, respectively. In this regime the thermal boundary layer expands to the entire domain. The minimum temperature in the domain is 0.394. However, the initial temperature inside the domain was set to 0. Therefore, the entire flow domain has been heated up and the thermal boundary layer is not distinct in this regime.

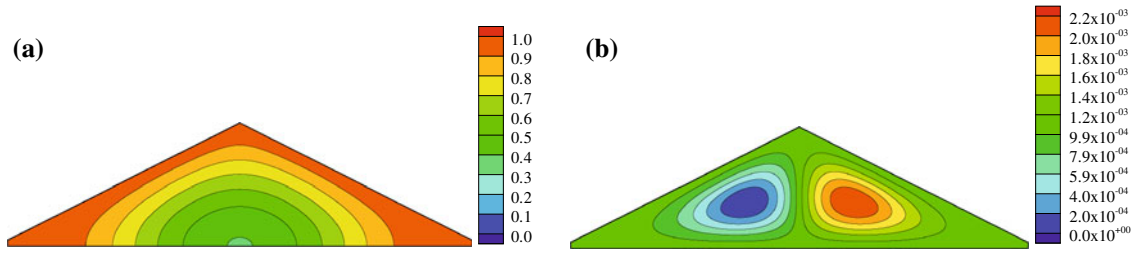

Fig. 7 **a** Temperature contours and **b** streamlines with $Pr = 0.72$, $Ra = 10$ and $A = 0.5$ at time $\tau/\tau_s = 0.156$

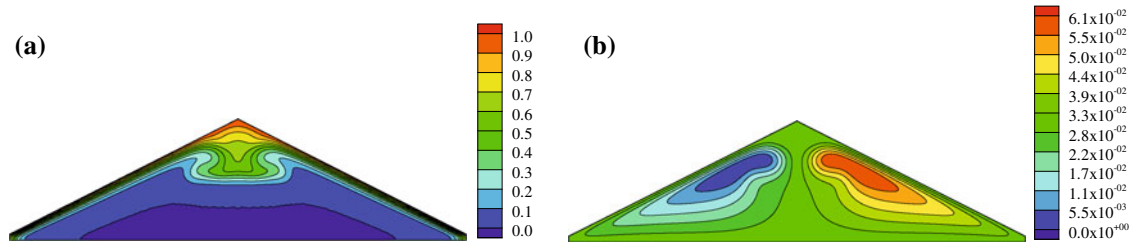

Fig. 8 **a** Temperature contours and **b** streamlines with $Pr = 0.72$, $Ra = 3.0 \times 10^6$ and $A = 0.5$ at time $\tau/\tau_s = 7.92 \times 10^{-3}$

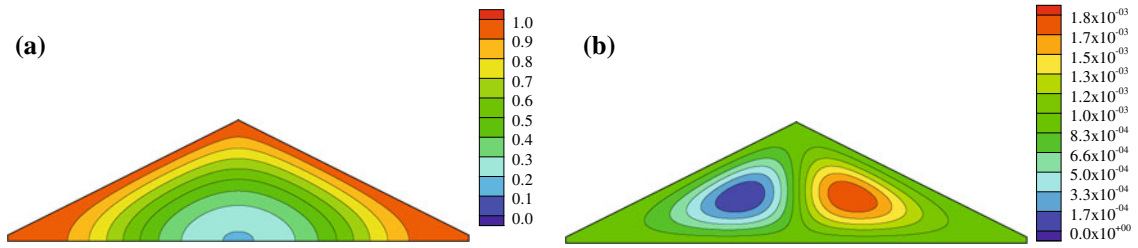

Fig. 9 **a** Temperature contours and **b** streamlines with $Pr = 0.72$, $Ra = 5.0$ and $A = 0.5$ at $\tau/\tau_{sr} = 0.147$

Moreover, there is no steady state of the flow inside the cavity as it continues to be heated up as time passes and may become isothermal. There are two cells in the streamlines on both sides of the center line of the attic where the direction of the left cell is clockwise and the right cell is anti-clockwise.

6.2 Convection regime

The numerical results of a relatively high Rayleigh number for this regime with $Pr = 0.72$, $Ra = 3.0 \times 10^6$ and $A = 0.5$ at $\tau/\tau_s = 7.92 \times 10^{-3}$ are given in Fig. 8 for the regime $Ra > (1 + Pr)(1 + A^2)/(A^2 Pr)$. The temperature contours are presented in Fig. 8a and the streamlines are presented in Fig. 8b. We notice that the convection increases significantly in this regime as the Rayleigh number increases. The steady state thermal boundary layers are distinct. The hot fluid travels through the boundary layers adjacent to both inclined walls and meet near the apex. The flow then has no other choice but to come downwards. However, the interior temperature is lower than the temperature in the downward flow. Therefore, the hot fluid on top and the cold fluid in the interior form a horizontal stratification. This stratification process eventually heats up the entire cavity.

7 Flow development in different regimes for ramp heating

7.1 Ramp time shorter than steady time

Figure 9 shows the temperature contours and the streamlines for $Pr = 0.72$, $Ra = 5.0$ and $A = 0.5$ at time $\tau/\tau_{sr} = 0.147$ for the regime $Ra < (1 + Pr)(1 + A^2)\, h^4/[A^2 Pr\kappa^2 t_p^2]$. The ramp time for this case is $\tau_p/\tau_{sr} = 3.68 \times 10^{-3}$. Figure 9a presents the temperature contours and Fig. 9b presents the corresponding streamlines. As soon as the heating starts the boundary layer develops and expands from the heated walls and reaches to the bottom surface. Two circular cells are seen in the streamlines

(Fig. 9b) with a clockwise circulation at the left side and an anti-clockwise circulation at the right side.

7.2 Ramp time longer than steady time

A representative Rayleigh number for this flow regime ($Ra > (1 + Pr)(1 + A^2)h^4/[A^2 Pr\kappa^2 t_p^2]$) has been chosen as $Ra = 6.0 \times 10^6$. The temperature contours and the stream lines have been shown in Fig. 10 at different times of the boundary layer development for aspect ratio $A = 0.5$. The ramp time, selected for this problem, is $\tau_p/\tau_{sr} = 1.57$.

The isotherms and stream lines of Fig. 10a, b are at $\tau/\tau_{sr} = 0.628$, which is the time before the flow becomes quasi-steady; Figure 10c, d are at $\tau/\tau_{sr} = 1.256$, when the flow is in quasi-steady mode; Fig. 10e, f are at the time when the ramp just finishes ($\tau/\tau_{sr} = 1.57$); and Fig. 10g, h are at time after the ramp is finished ($\tau/\tau_{sr} = 3.14$). It is seen clearly from these figures that initially the boundary layer develops adjacent to the inclined walls of the cavity and moves upwards. However, as time passes, the top of the cavity gradually fills with hot fluid and becomes stratified, where the top portion fluid is hotter than the bottom portion. At the end the entire cavity has been heated up. It is noted that the typical situation of quasi-steady state and the finishing time of ramp cannot be identified from these set of isotherms and streamlines.

8 Validation of selected scales

The flow features discussed theoretically above are verified on the basis of a complete series of numerical simulations. It is assumed that the fluid contained in the attic space is originally motionless and of a uniform temperature $\theta = 0$. The cavity is heated from the top by means of sudden and ramp heating boundary conditions of the sloping wall. Throughout this simulation, the horizontal bottom wall is assumed to be adiabatic. The above scales have been developed with an assumption that the flow is symmetric along the symmetry center line of the cavity. Previous

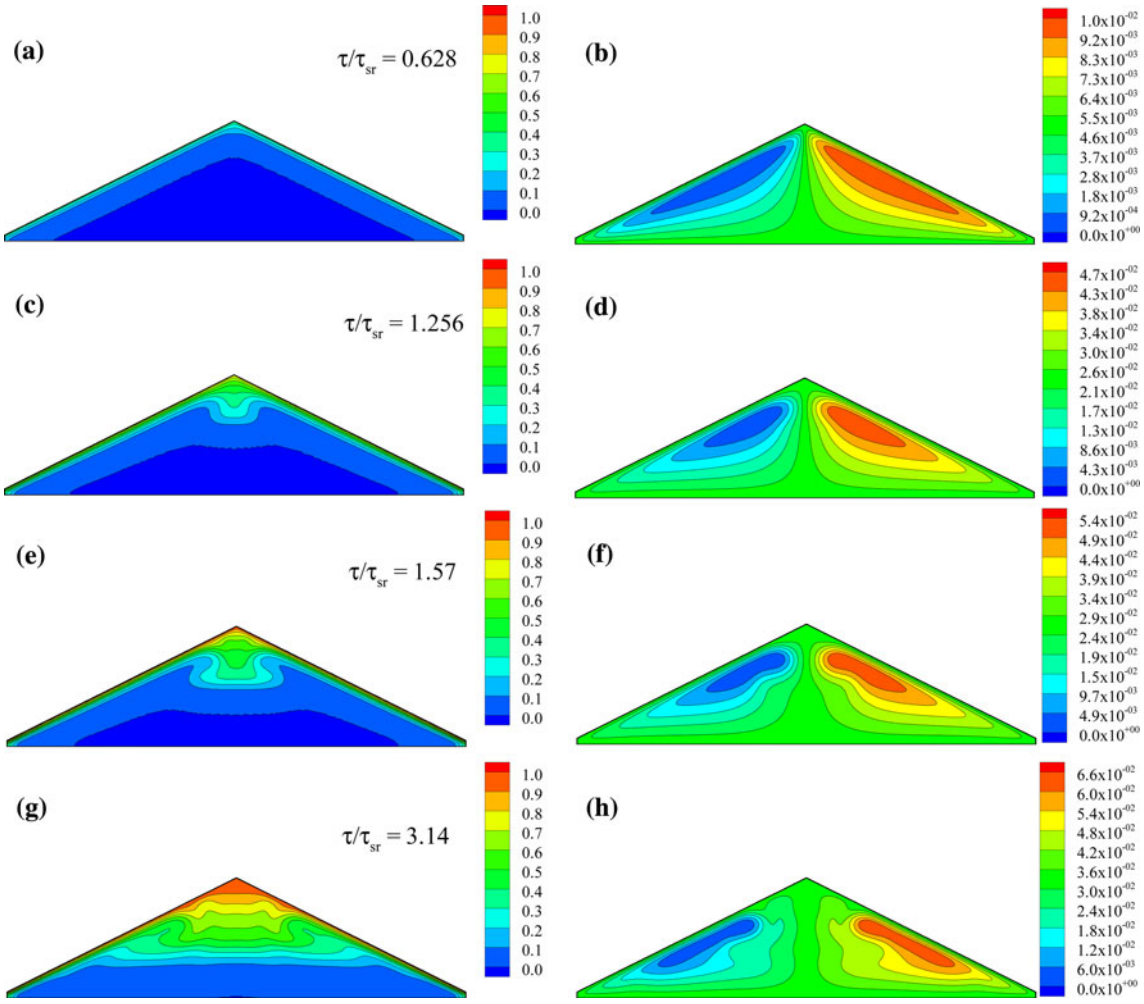

Fig. 10 Temperature contours (**a**, **c**, **e**, **g**) and streamlines (**b**, **d**, **f**, **h**) with $Pr = 0.72$, $Ra = 6.0 \times 10^6$ and $A = 0.5$ at different times

Table 4 Values of A and Ra for six runs for sudden heating

Runs	A	Ra
1	0.5	1.5×10^7
2	0.5	3.0×10^6
3	0.5	1.5×10^6
4	0.5	6.0×10^5
5	0.2	3.0×10^6
6	1.0	3.0×10^6

studies of attic space have revealed that the flow is indeed symmetric along the center line for the case of heating on the sloping walls.

The detailed validation of the boundary layer development has been discussed in Saha, et al. [12] (e.g. velocity scale, thickness scale etc.). For brevity, those results are not repeated here. However, heat transfer scales together with steady state time scales have been verified in this study. Moreover, the heating-up time scale and the subsequent heat transfer scale at that time have also been verified.

8.1 Sudden heating

The heating-up time is determined by the heat flux through the natural convection boundary layer. The hot fluid moves upward along the boundary layers of both inclined walls and meets under the apex of the enclosure. Then it has no choice but to move downward right below the tip, forming a horizontal stratification. This stratified hot fluid fills the enclosure, ultimately reaching the bottom surface at which time the whole enclosure is filled with hot fluid.

In Table 4, Runs 1–4 with $Ra = 1.5 \times 10^7$, 3.0×10^6, 1.5×10^6 and 6.0×10^5 while keeping $A = 0.5$ and $Pr = 0.72$ unchanged have been carried out to show the dependence of the scaling relations on the Rayleigh number, Ra; Runs 5–6 and 2 with $A = 0.2$, 1.0 and 0.5, respectively, while keeping $Ra = 3.0 \times 10^6$ and $Pr = 0.72$ unchanged have been carried out to show the dependence on the slope of the inclination of the plate. All Rayleigh numbers considered here are in the convection regime.

The numerical results showing the dependence of the instantaneous average Nusselt number Nu on Ra, and A at the boundary-layer development stage and at the heating-up stage are, respectively, presented in Figs. 11 and 12. Figure 11a shows the raw data of the time series of the Nusselt number which have been calculated from the left inclined wall of the cavity for different Rayleigh numbers and aspect ratios. It is found that the Nusselt number depends strongly on Ra and A. In Fig. 11b, the time has been normalized with respect to the steady state time of the boundary layer development. We notice that the steady state of the Nusselt numbers fall on a vertical line (long dashed line), which validates the steady state time scale of the boundary layer development (63). The normalized Nusselt number with respect to its steady state value is plotted against normalized time with respect to the steady state time scale in Fig. 11c. As anticipated, all lines

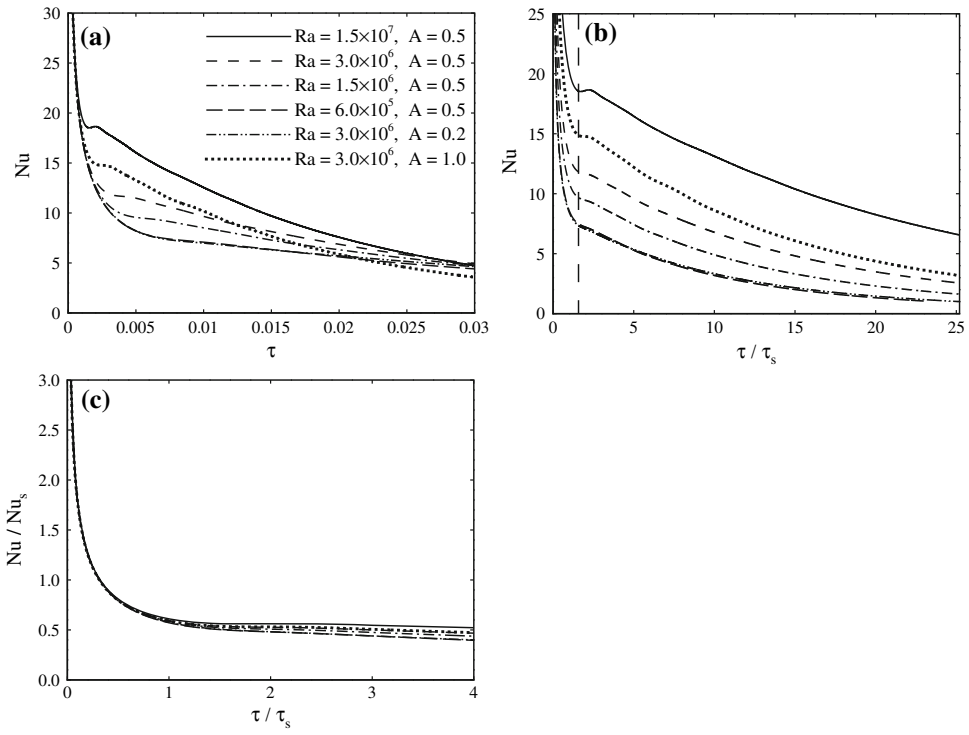

Fig. 11 Time series of the average Nusselt number calculated on the left inclined wall. **a** Plot of raw data; **b** Nusselt number versus normalized time; and **c** Normalized Nusselt number versus normalized time

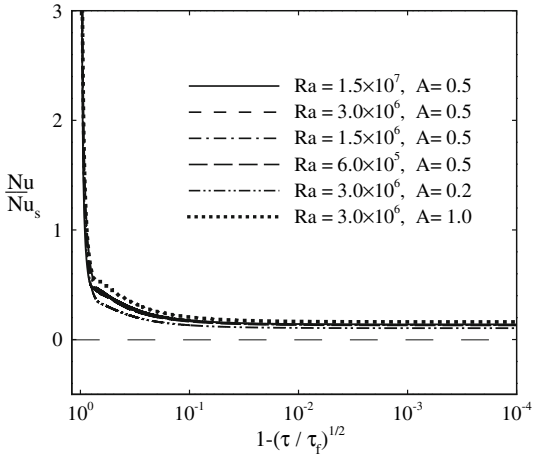

Fig. 12 Time series of Nusselt number on the left inclined wall for heating-up stage for sudden heating for six runs

collapse together in one line which confirms the scaling relation (13) at the boundary-layer development stage.

The Nusselt number at the heating up time has been plotted in Fig. 12. Again all lines collapse on a single line which validates the scaling relation (67) at the heating up stage. Note that the x-axis is on a log scale.

To verify the heating-up time scale, the temperature has been recorded at the midpoint of the bottom surface, which is shown in Fig. 13. Raw data of the time series of the temperature for different Rayleigh numbers and aspect ratios are plotted in Fig. 13a. It is anticipated that initially there is no response of the temperature at the middle point of the bottom surface. As soon as the hot fluid comes from the top and reaches the bottom, the temperature starts to increase. However, this response time is different for different Ra and A. In Fig. 13b, the time is normalized with respect to the heating-up time (66) and the temperature has been normalized by the temperature difference. We see that the temperature series response at the same time for different flow parameters. This confirms that the heating-up time scale (66) is accurate.

8.2 Ramp heating

Similarly to the sudden heating case, the heating-up time is also determined by the heat flux through the natural convection boundary layer for the ramp temperature boundary condition. Table 5 shows the full sets of flow cases considered for the numerical simulation. All Rayleigh numbers considered here are in the regime where the ramp time is longer than the quasi-steady time.

To demonstrate the dependency of the Nusselt number on time at various stages of boundary development stage, the time series of Nusselt number on the left inclined surface of the attic space is plotted in Fig. 14. It is seen in Fig. 14a that it increases with time and becomes quasi-steady state at about 2.26×10^{-3}. Since the surface is still receiving heat from the ramp temperature boundary condition, the Nusselt number increases until the ramp is finished. After the ramp finishes it suddenly drops and decreases as time increases. We have seen that the Nusselt number scale at the initial stage is the order of $O(\tau^{1/2})$ (see Eq. 35). Therefore, in Fig. 14b the Nusselt number is plotted against $\tau^{1/2}$ and shows an initial linear growth. However, the Nusselt number scale after the quasi-steady state is of the order $O(\tau^{5/4})$ (see Eq. 37). To verify this scale, the Nusselt number in Fig. 14c is plotted against $\tau^{5/4}$. The figure shows that after the quasi-steady state the Nusselt number show a linear growth until the ramp is finished.

The numerical results showing the dependence of the average Nusselt number, Nu on Ra, and A at the boundary-layer development stage are presented in Figs. 15 and 16. The Nusselt number has been calculated in two different ways; one with reference to the maximum temperature difference (see Eq. 74) and the other

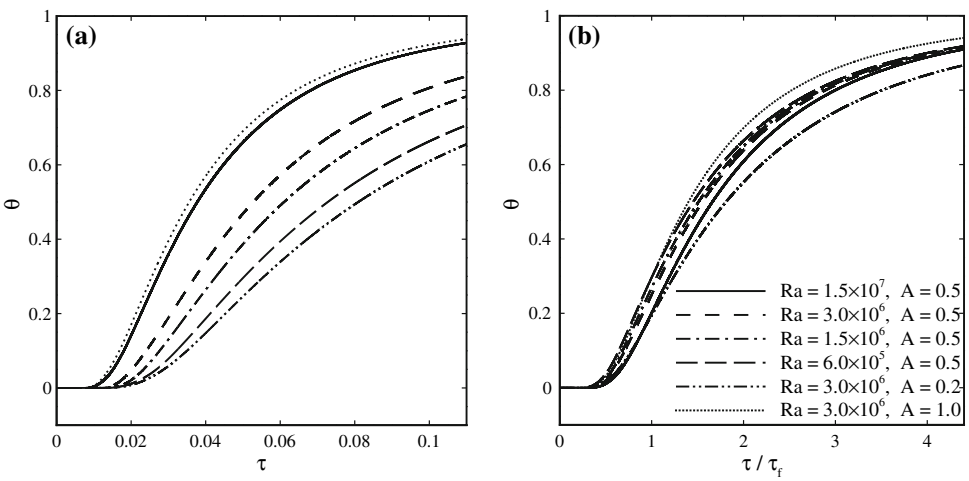

Fig. 13 Time series of temperature recorded on the midpoint of the bottom surface. **a** Plot of raw data; **b** Normalized temperature versus normalized time for sudden heating for six runs

Table 5 Values of A and Ra for the six runs for ramp heating

Runs	A	Ra
1	0.5	3.0×10^7
2	0.5	1.5×10^7
3	0.5	6.0×10^6
4	0.5	3.0×10^6
5	1.0	3.0×10^7
6	0.2	3.0×10^7

with reference to the instantaneous temperature difference (see Eq. 76). Figure 15a shows the raw data of the time series of the Nusselt number which has been calculated from the left inclined wall of the cavity using the maximum temperature difference for different Rayleigh numbers and aspect ratios. It is found the Nusselt number depends strongly on Ra and A. In Fig. 15b, the time has been normalized with respect to the quasi-steady time (69) and Nusselt number has been normalized by the scaling value (74). It is clear that all lines collapse together until the ramp is finished which validates the quasi-steady time (69) and Nusselt number (74) scales of the boundary-layer development stage.

In Fig. 16, the Nusselt number has been calculated using the instantaneous temperature difference (τ/τ_p for $\tau \leq \tau_p$). Raw data of the time series of the Nusselt number is plotted in Fig. 16a. It is seen that initially the Nusselt number approaches infinity and decreases sharply until the quasi-steady state time. After the quasi-steady state it increases very slowly until the ramp is finished. After the ramp finishes, the Nusselt number again decreases very fast. In Fig. 16b, the time has been normalized by (69) and the Nusselt number by (76). Again all lines lie together until the ramp is finished, which confirms the scaling relation (69) and (76).

The Nusselt number at the heating-up time is plotted in Fig. 17. Again all lines fall together in a line which validates the scaling relation (79) at the heating up stage. Note that the x-axis is on a log scale.

To verify the heating-up time scale, the temperature has been recorded at the middle point of the bottom surface and plotted in Fig. 18. Raw data of the time series of the temperature for different Rayleigh numbers and aspect ratios has been shown in Fig. 18a. It is anticipated that initially there is no response of the temperature at the middle point of the bottom surface. As soon as the hot fluid comes from the top and reaches the

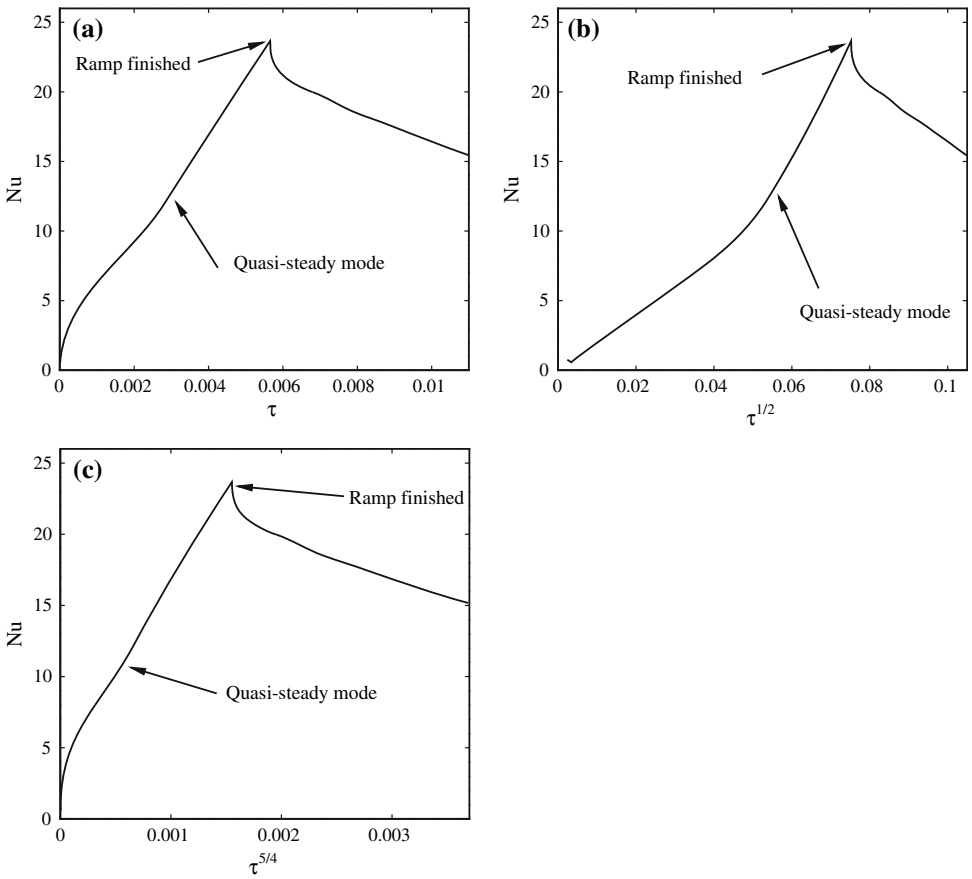

Fig. 14 Time series of total heat flux on the left inclined surface for $Ra = 4.0 \times 10^7$, $A = 0.5$ and $Pr = 0.72$

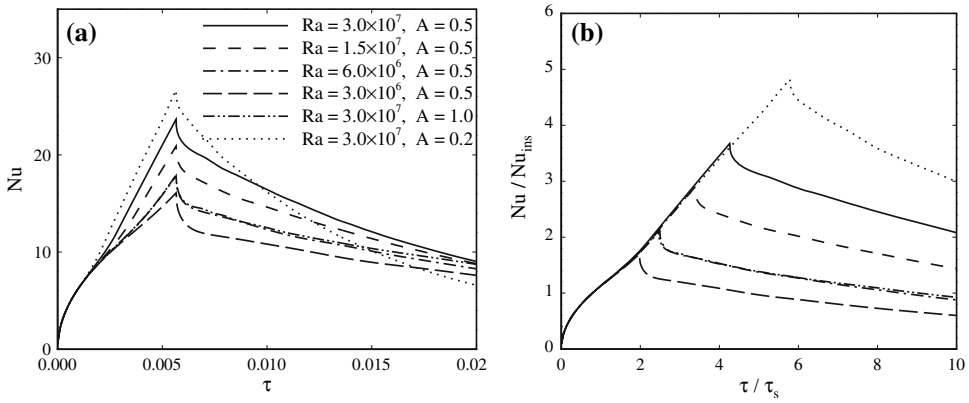

Fig. 15 Time series of the average Nusselt number calculated on the left inclined wall. **a** Plot of raw data; **b** Normalized Nusselt number versus normalized time for ramp heating for six runs

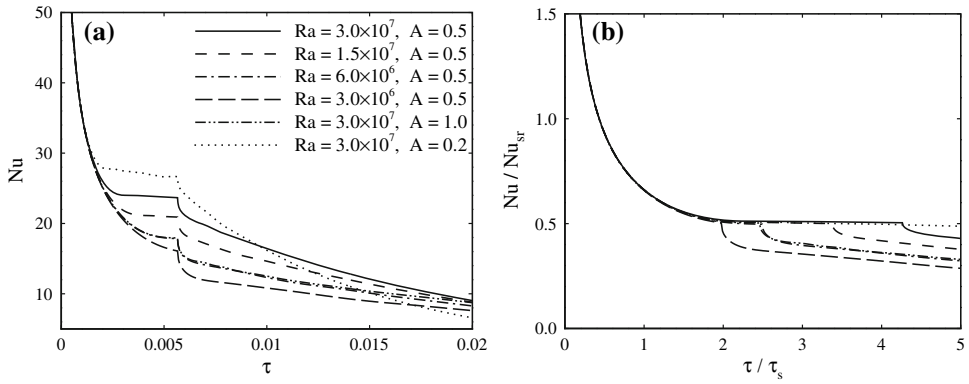

Fig. 16 Time series of the average Nusselt number calculated on the left inclined wall. **a** Plot of raw data; **b** Normalized Nusselt number versus normalized time for ramp heating for six runs

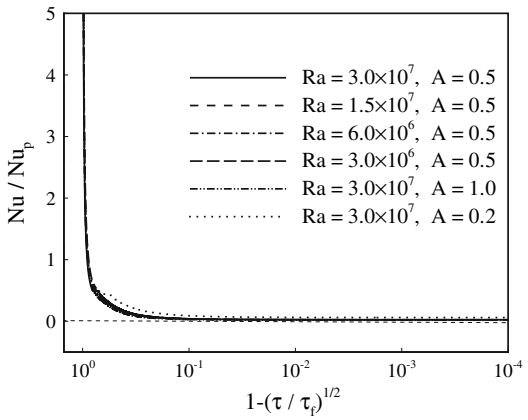

Fig. 17 Normalized time series of Nusselt number at the heating up stage on the left inclined wall of the cavity for ramp heating for six runs

bottom, the temperature starts to increase. However, this response time is different for different values of *Ra* and *A*. In Fig. 18b, the time is normalized with respect to the heating-up time (77) and the temperature has been normalized by the temperature difference. We see that the temperature starts to rise at the same time for different flow parameters. This confirms that the heating-up time scale (77) is accurate.

9 Summary

Natural convection adjacent to heated inclined walls of an attic space is examined by scaling analysis and the scales verified by numerical simulation for air ($Pr = 0.72$). It is found that the flow is mainly dominated by four distinct stages for the sudden heating boundary condition, i.e. start-up stage, transitional stage, steady state stage and heating-up stage. The scaling relations are formed based on the established characteristic flow parameters of the maximum velocity inside the boundary layer (u_s), the time for the boundary layer to reach the steady state (t_s), the thermal (δ_T) and viscous (δ_v) boundary layer thicknesses, Nusselt number scale (Nu_s), the heating up time (t_f) and the Nusselt number at the heating-up time. Moreover, some important regimes based on the Rayleigh number have been established in this investigation. The scaling results agree very well with the numerical simulations.

Furthermore, a temperature boundary condition of a ramp function applied to the inclined walls has also been investigated. The boundary layer flow for this boundary condition depends on the comparison of the time at which the ramp heating is completed with the time at which the boundary layer completes its growth. If the ramp time is long compared with the steady state time, the thermal boundary layer reaches a quasi-steady mode in which the

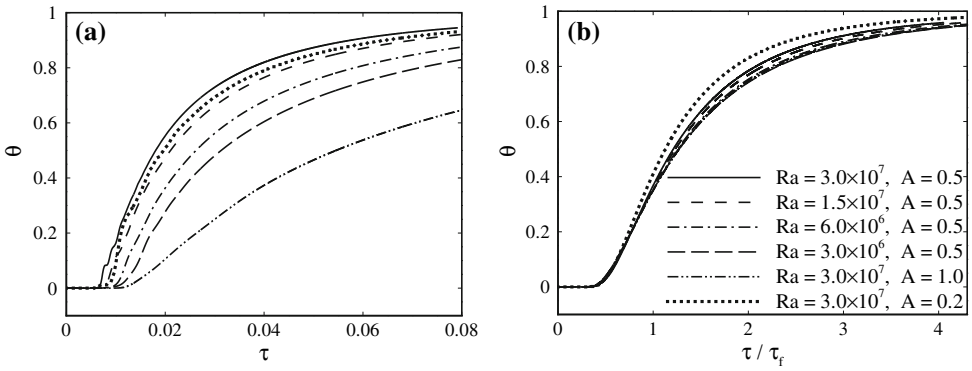

Fig. 18 Time series of temperature recorded on the midpoint of the bottom surface. **a** Plot of raw data; **b** Normalized temperature versus normalized time for ramp heating for six runs

growth of the layer is governed by the thermal balance between convection and conduction. On the other hand, if the ramp is completed before the thermal boundary layer becomes steady, the subsequent growth is governed by the balance between buoyancy and inertia, as for the case of instantaneous heating. Several scaling relations have been established in this study, which include the maximum velocity parallel to the inclined plate inside the boundary layer (u_{sr}), the time for the boundary layer to reach the quasi-steady state (t_{sr}) and the thermal and viscous boundary layer thicknesses (δ_T rand δ_v), Nusselt number scale (Nu_{sr} and Nu_{ins}), the heating up time (t_f) and the Nusselt number at the heating-up time. Like the sudden heating case, some important flow regimes have been established for the ramp heating boundary condition. The scaling results agree very well with the numerical simulations. The comparisons between the scaling relationships and the numerical simulations demonstrate that the scaling results agree very well with the numerical simulations.

Acknowledgments This work was funded by the Australian Research Council (ARC).

References

1. Flack RD (1980) The experimental measurement of natural convection heat transfer in triangular enclosures heated or cooled from bellow. ASME J Heat Transf 102:770–772
2. Akinsete VA, Coleman TA (1982) Heat transfer by steady laminar free convection in triangular enclosures. Int J Heat Mass Transf 25:991–998
3. Asan H, Namli L (2000) Laminar natural convection in a pitched roof of triangular cross-section: summer day boundary conditions. Energy Buildings 33:69–73
4. Poulikakos D, Bejan A (1983) The fluid dynamics of an attic space. J Fluid Mech 131:251–269
5. Lin W, Armfield SW, Patterson JC (2008) Unsteady natural convection boundary-layer flow of a linearly stratified fluid with $Pr < 1$ on an evenly heated semi-infinite vertical plate. Int J Heat Mass Transf 51:327–343
6. Lin W, Armfield SW, Patterson JC (2007) Cooling of a $Pr < 1$ fluid in a rectangular container. J Fluid Mech 574:85–108
7. Lin W, Armfield SW (2005) Scaling laws for unsteady natural convection cooling of fluid with $Pr < 1$ in a vertical cylinder. Phys Rev E 72:016306
8. Lin W, Armfield SW (2005) Unsteady natural convection on an evenly heated vertical plate for $Pr < 1$. Phys Rev E 72:066309
9. Lei C, Patterson JC (2002) Unsteady natural convection in a triangular enclosure induced by absorption of radiation. J Fluid Mech 460:181–209
10. Lei C, Patterson JC (2005) Unsteady natural convection in a triangular enclosure induced by surface cooling. Int J Heat Fluid Flow 26:307–321
11. Patterson JC, Lei C, Armfield SW, Lin W (2009) Scaling of unsteady natural convection boundary layers with a non-instantaneous initiation. Int J Therm Sci 48:1843–1852
12. Saha SC, Patterson JC, Lei C (2010) Natural convection boundary layer adjacent to an inclined flat plate subject to sudden and ramp heating. Int J Therm Sci. doi:10.1016/j.ijthermalsci.2010.03.017
13. Saha SC, Patterson JC, Lei C (2010) Natural convection in attics subject to instantaneous and ramp cooling boundary conditions. Energy Building. doi:10.1016/j.enbuild.2010.02.010
14. Leonard BP, Mokhtari S (1990) ULTRA-SHARP nonoscillatory convection schemes for high-speed steady multidimensional flow. NASA TM 1-2568 (ICOMP-90-12), NASA Lewis Research Centre
15. Patterson JC, Armfield SW (1990) Transient features of natural convections in a cavity. J Fluid Mech 219:469–497